ACS APPLIED ENERGY MATERIALS

www.acsaem.org Article

Switchable Color Semiconductors: Methylamine Intercalation, Deintercalation, and Retention in Two-Dimensional Halide Perovskites

Josephine L. Surel, Elizabeth V. Cutlip, James R. Mandeville, and Jeffrey A. Christians*

Cite This: *ACS Appl. Energy Mater.* 2022, 5, 12029−12038 Read Online

ACCESS | Metrics & More | Article Recommendations | Supporting Information

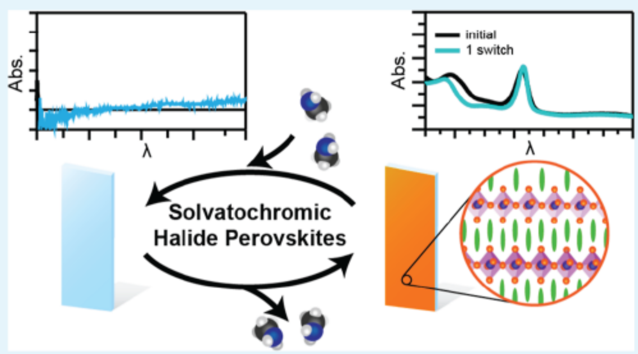

ABSTRACT: The low formation energy of metal halide perovskites (MHPs) and their high performance in optoelectronic applications make them rather interesting semiconductor materials. In this work, we take advantage of the tunability of two-dimensional (2D) halide perovskites of the type A_2PbI_4 to explore a chromogenic mechanism in these materials where methylamine is allowed to intercalate into and deintercalate from the halide perovskite films. Methylamine intercalation results in a change in color from the initial yellow/orange color of the A_2PbI_4 films to visibly transparent films, while deintercalation leads to a return of a colored film. The reversibility of this solvatochromic mechanism was found to be highly dependent on the nature of the A-site cation used. We observe the formation of iodoplumbate phases, mixed 2D/three-dimensional (3D) perovskites, and/or 3D perovskites as secondary phases formed in some systems and, by exploring a wide array of A_2PbI_4 materials, we identify key design rules for the A-site cation to limit secondary phase formation and structural changes associated with methylamine intercalation/deintercalation. Specifically, the effects of changing cation−cation, cation "head"-inorganic, and cation "tail"-inorganic interactions in this system are demonstrated. By carefully controlling these interactions, more robust solvatochromic systems are realized. These initial explorations of metal halide solvatochromism improve the understanding of A-site cation design in A_2PbI_4 MHPs and show that these are a promising class of solvatochromic semiconductors.

KEYWORDS: *chromogen, halide perovskites, two-dimensional, methylamine, semiconductors, color change*

■ INTRODUCTION

Metal halide perovskites (MHPs) and an even wider array of perovskite-inspired materials have been explored in recent years for their interesting properties and suitability to a wide range of devices and applications.[1−8] MHPs are a class of semiconductors with AMX_3 stoichiometry, which structurally consist of corner-sharing $[MX_6]^{2-}$ octahedra ($M = Pb^{2+}$, Sn^{2+}, *etc.*; $X = I^-$, Br^-, Cl^-) with an A-site cation supporting this M−X framework; however, within this general structural motif, MHPs exhibit considerable flexibility.[9,10] For example, the A-site cation can be an alkali metal or small organic cation (A = Cs^+, methylammonium, or formamidinium) and form an extended three-dimensional (3D) network of corner-sharing $[MX_6]^{2-}$ octahedra, or two-dimensional (2D) networks of $[MX_6]^{2-}$ octahedra can be formed, separated by a layer of the A-site cation, as in Ruddlesden−Popper and Dion−Jacobson phases.[10,11] In Ruddlesden−Popper MHPs, the materials have the general formula $A'_2A_{n-1}M_nX_{3n+1}$, where A and A′ are 1+ cations, and n (n = 1, 2, 3,... ∞) indicates the number of connected $[MX_6]^{2-}$ octahedral sheets within each metal halide

The rather unique combination of low-temperature processing, long charge carrier diffusion lengths, tunable optical absorption, and defect tolerance has enabled MHP solar cells with power conversion efficiencies >25% and[12] light-emitting diodes (LEDs) with quantum efficiencies >20%[8] and spurred interest for a range of other optoelectronic applications, such as gas sensing,[3] radiation detection,[6] neuromorphic computing,[4] and spin-polarized LEDs.[5] While most inorganic semiconductors are unable to change their optical properties on demand, MHPs can be chromogenic. Chromogenic materials are materials that change color state under the action of external stimuli (*e.g.*, temperature, light, electric potential, and solvent/vapor). In MHPs, chromogenic behavior can be achieved through gas intercalation[3,7,13,14] or

Received: May 3, 2022
Accepted: September 1, 2022
Published: September 14, 2022

https://doi.org/10.1021/acsaem.2c01352
ACS Appl. Energy Mater. 2022, 5, 12029−12038

crystal phase transformations,[15] with some MHPs showing multicolor chromism.[16] When combined with the excellent optoelectronic properties of MHPs, chromogenic behavior has the potential to unlock exciting new functionalities. For example, an initial demonstration by Wheeler *et al.* has shown a high power conversion efficiency (>11%) photovoltaic window, which could dynamically switch its visible light transmittance between a power-producing dark state, and a highly transparent state, which performed well as a window.[7] In photovoltaic windows, a controllable color change could allow the device to avoid the tradeoffs between power production and visible transmittance[17] but, more generally, dynamic control of semiconductor properties could enable new applications.

One interesting chromogenic mechanism is the intercalation of solvent molecules, termed solvatochromism. Intercalation of solvent molecules into the MHP structure can readily occur. Early work by Saparov and Mitzi demonstrated that pentafluorophenethylammonium-based $(C_6F_5C_2H_4NH_3)_2SnI_4$ 2D perovskites could effectively intercalate aryl compounds into the organic cation bilayers, forming new crystalline materials.[9] Later, the intercalation−deintercalation of water molecules was found to cause methylammonium lead iodide ($MAPbI_3$) to change from dark to clear.[13,14,18] The switchable photovoltaic window reported by Wheeler *et al.* utilized the intercalation−deintercalation of methylamine (MA) in $MAPbI_3$ to control the color state.[7] For solvatochromic systems, a key challenge is the development of solvents to reversibly intercalate and deintercalate without degrading the MHP. This represents a key challenge for applications of these systems. For example, while water can reversibly hydrate dark brown/black $MAPbI_3$ and form the colorless hydrate $MAPbI_3 \cdot H_2O$,[14] significant recrystallization occurs and exposure to light results in the irreversible degradation to PbI_2.[13] Similarly, intercalation of methylamine gas into $MAPbI_3$ generates the colorless material $MAPbI_3 \cdot xCH_3NH_2$ but leaves significant structural changes upon deintercalation.[7,19]

The templating effects of the A-site cation have been explored in MHPs for 30 years,[11,20] proving to be a useful tool for controlling the structure and tuning properties.[9] In this work, we utilize A_2PbI_4 MHPs and explore the solvatochromism of these materials with MA. This A_2PbI_4 stoichiometry is typical of Ruddlesden−Popper phase halide perovskites, but the exact structure is dependent on the A-site cation used.[21] We find that the reversibility of solvatochromism in these MHPs is highly dependent on the A-site material used, with the primary irreversibility being incomplete MA deintercalation and also the volatility of the deprotonated A-site cations. When MA is retained in the films and does not fully deintercalate, we observe a variety of secondary phases that form depending on the amount of MA that remains within the A_2PbI_4 films. The wide tunability of 2D MHPs offers an interesting materials design aspect for tuning solvatochromic semiconductor properties and improving the reversibility of this color change mechanism. We explore a selected subset of this material space to begin to understand design rules for solvatochromic MHPs. Modulating the intermolecular forces occurring in the organic A-site interlayer, the $NH_3 \cdots I$ hydrogen bonding interactions between the interlayer and inorganic perovskite sheets, and the organic "tail" and perovskite sheets allow for the control and reduction of secondary phase

EXPERIMENTAL DETAILS

Materials. Ammonium halide salts and fluorine-doped tin oxide glass substrates were purchased from Greatcell Solar Materials and used as received. Lead (II) iodide (99.9985% metals basis) was purchased from Alfa Aesar. All other chemicals were purchased from Sigma-Aldrich and used as received.

Synthesis of Phenbutylammonium Iodide. Phenbutylammonium iodide was synthesized by adapting a previously demonstrated procedure for phenethylammonium iodide synthesis.[22] First, 12 mmol 4-phenbutylamine was combined with 2 mL of ethanol and cooled with a salted ice bath. Concentrated HI (57 wt.% in water) was slowly added dropwise in slight excess (∼13 mmol), and a precipitate was formed. The precipitate was washed with cold diethyl ether and filtered using vacuum filtration to remove excess iodide. The remaining white solid was then dissolved in the minimum amount of hot (60 °C) isopropanol and then cooled to −10 °C in order to recrystallize. The crystals were washed again with vacuum filtration and cold isopropanol and allowed to dry completely before use.

Synthesis of 4-Iodophenethylammonium Iodide. 4-Iodophenethylammonium iodide was synthesized similar to phenbutylammonium iodide. First, 4 mmol 4-iodo-phenethylamine was combined with 667 μL of ethanol and cooled with a salted ice bath. Concentrated HI (57 wt.% in water) was slowly added dropwise in slight excess (∼4.5 mmol), and a precipitate was formed. The precipitate was washed with cold diethyl ether and filtered using vacuum filtration to remove excess iodide. The remaining yellow solid was then dissolved in the minimum amount of hot (∼60 °C) isopropanol and then cooled to ∼0 °C. Cold diethyl ether was added to precipitate the compound fully, and then the white solid was isolated by vacuum filtration.

Preparation of A_2PbX_4 Films. To fabricate halide perovskites with the general formula A_2PbX_4, a similar method was used for each A site: ethylammonium ($CH_3CH_2NH_3^+$, EA), phenethylammonium ($C_6H_5C_2H_4NH_3^+$, PEA), 4-fluorophenethylammonium ($FC_6H_4C_2H_4NH_3^+$, F-PEA), 4-chlorophenethylammonium ($ClC_6H_4C_2H_4NH_3^+$, Cl-PEA), 4-iodophenethylammonium ($IC_6H_4C_2H_4NH_3^+$, I-PEA), 4-methoxyphenethylammonium ($CH_3OC_6H_4C_2H_4NH_3^+$, MeO-PEA), 4-hydroxyphenethylammonium ($HOC_6H_4C_2H_4NH_3^+$, HO-PEA), phenbutylammonium ($C_6H_5C_4H_8NH_3^+$, PBA), *n*-pentylammonium ($CH_3(CH_2)_4NH_3^+$, *n*-PA), 4-methoxyphenylammonium ($CH_3OC_6H_4NH_3^+$, MeO-PhA), and phenylammonium ($C_6H_5NH_3^+$, PhA).

Precursor solutions were prepared in a mixed solvent of dimethyl sulfoxide (DMSO) and dimethylformamide (DMF). A ratio of 2 mmol AI (where AI is one of the iodide salts of the ammonium cations listed above), 1 mmol PbI_2, and 1 mmol DMSO were added to 600 mg of DMF and mixed vigorously until the solids were completely dissolved. These precursor solutions were then diluted by the addition of DMF to fabricate thinner films, depending on the desired optical density for a specific experiment (*e.g.*, 1:10 v/v for some absorption experiments, 1:3 v/v for SEM imaging of morphology). Fluorine-doped tin oxide (FTO) glass substrates (2.5 × 2.5 cm, TEC7) were cleaned by sonication in a soap solution for 10 min and then in isopropanol for an additional 10 min. Just before film deposition, the substrates were cleaned using a UV−ozone cleaner for 10 min. Perovskite film deposition was carried out in a nitrogen purge box with a relative humidity of less than 10%. Approximately 40 μL of the precursor solution was spread onto the FTO substrate and then coated by spin coating at 4000 rpm for 25 s. With 15 s remaining, 200 μL of toluene antisolvent was dripped onto the center of the substrate.[23] For some AI salts and thicker films, the precise timing and volume of antisolvent were changed slightly to achieve more specular films; toluene volume ranged from 200 to 500 μL, and drip time ranged from 15 to 17 s remaining. Films that were not diluted at all with DMF exhibited significant scattering. Following spin coating, the films were annealed on a hotplate at 110 °C for 10 min.

***In Situ* Absorption Measurements.** Absorption kinetics measurements were taken using an Ocean Insight Flame-T spectrophotometer and a tungsten halogen light source (HL-2000-

https://doi.org/10.1021/acsaem.2c01352
ACS Appl. Energy Mater. 2022, 5, 12029−12038

LL). Films were measured in a sealed cuvette. To expose the film to MA vapor, N_2 was slowly bubbled through an MA solution and introduced into the cuvette atmosphere. Using a 3-way valve, the cuvette atmosphere could be rapidly changed to pure N_2.

MA Vapor Switching. To switch the perovskite films using MA, the film was placed at the bottom of a gas wash chamber. To expose the film to MA vapor, N_2 was slowly bubbled through a solution of MA in ethanol and introduced into the gas wash chamber until the sample turned completely colorless. The flow was then switched to pure N_2 using a 3-way valve, and the chamber was purged with N_2 until the film changed back to a dark shade. We define one cycle of this color change process (*viz.*, exposure of the film to MA gas to turn the film clear and then removal of the MA gas) as a switch.

While in most of the experiments presented, moisture was present (at some level) during the described experiments, in specific experiments, as discussed in the article, we took additional care to ensure that the system was moisture-free throughout the process by using fresh, anhydrous methylamine solution and purging the entire system with nitrogen for an extended period before beginning.

Additionally, the perovskite films were switched by placing them briefly over the top of a vial of MA solution and then removing them. This method led to larger variation in MA exposure (not all portions of the films changed color, or some portions were exposed to too much MA) and so was only used for the multiple switch experiments presented in the Supporting Information.

Characterization. UV–visible absorption spectroscopy (steady-state) measurements were conducted using a Cary 50 UV-VIS spectrophotometer. X-ray diffraction (XRD) measurements of the samples were performed with a Rigaku MiniFlex powder X-ray diffractometer using a Cu Kα source and a step size of 0.03°. ^{1}H NMR spectra were obtained on a Bruker Avance III 400 MHz spectrometer using standard acquisition parameters. Scanning electron micrographs were obtained using a JEOL JSM-IT700HR FESEM imaging using a 5 kV accelerating voltage and a secondary electron detector.

■ RESULTS AND DISCUSSION

Exploring the Solvatochromism of PEA_2PbI_4 and Methylamine. Initial investigations were centered on the 2D halide perovskite PEA lead iodide, PEA_2PbI_4.[22] PEA_2PbI_4 readily forms layered two-dimensional perovskite structures, referred to as a 2D perovskite.[10,11] To study the interactions between 2D perovskites and MA vapor, PEA_2PbI_4 films were exposed to MA gas by slowly bubbling nitrogen through a solution of MA in ethanol and then exposing the film to this gas stream, as described in the Experimental Details. As has been shown for $MAPbI_3$,[7] MA intercalates into the perovskite material and causes the film to become visibly transparent. Then, to deintercalate MA, the gas sweeping the system was changed from the MA/N_2 mixture to pure N_2. This leads to deintercalation of MA from the film and a change from visibly transparent to a visibly colored film. Herein, we refer to this intercalation/deintercalation process as a "switch" because the color switches from colored to clear and back to colored. A schematic of this process is shown in Figure 1, and in some cases, we perform multiple cycles of intercalation/deintercalation as indicated [*e.g.*, *m* switch(es), *m* = 1, 2, 3...]. Figure 2 shows *in situ* absorption measurements that were taken during MA intercalation/deintercalation of PEA_2PbI_4. Figure 2A shows XRD measurements of the films initially and after a color switch compared to other materials.

PEA_2PbI_4 films were seen to bleach rapidly upon MA exposure, with the kinetics of this bleaching convoluted with the kinetics of gas exposure (Figure 2B, inset). Removing MA from the gas stream, there is a fast (~5–15 s) recovery of the ... nding to the reformation

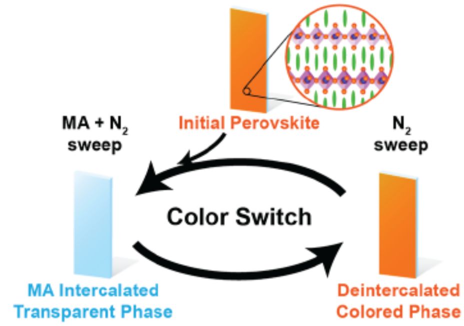

Figure 1. Color switch scheme. Basic schematic showing the process for MA intercalation/deintercalation used in this study. Throughout this article, this process is called a "switch" for shorthand.

of PEA_2PbI_4. In addition, there is the appearance of a new peak at ~545 nm, indicating the formation of $(PEA)_2MAPb_2I_7$ $[(A)_2A'_{n-1}B_nX_{3n+1}$ with $n = 2]$. This provides evidence that a rather significant amount of MA remains incorporated into the perovskite structure. The formation of this $n = 2$ phase requires that the following generic proton exchange reaction between the ammonium cation ($R-NH_3^+$) and methylamine, shown in eq 1, takes place in the films.

$$R - NH_3^+ + CH_3NH_2 \leftrightarrow R - NH_2 + CH_3NH_3^+ \quad (1)$$

As the film is swept with N_2 gas, MA continues to deintercalate, and some of $(PEA)_2MAPb_2I_7$ converts back into PEA_2PbI_4, as seen by the decrease in absorption at 545 nm (n = 2 phase) and continued growth of the absorption at 510 nm (n = 1) (Figure 2C and inset), with the reaction in eq 1 proceeding in reverse. This interpretation is supported by XRD analysis (Figure 2A). In the switched film, the primary XRD peaks are associated with the (00*l*) peaks of n = 1 PEA_2PbI_4 [*viz.*, (001) peak at 5.47°, (002) peak at 10.90°, *etc.*], but there are also new XRD peaks that correspond to the n = 2 phase $(PEA)_2MAPb_2I_7$, for example the peaks at 7.96° and 11.95° correspond to the (002) and (003) reflections of this phase.[24] However, the decay kinetics of $(PEA)_2MAPb_2I_7$ absorption are not identical to the growth kinetics of PEA_2PbI_4. Interestingly, we do not see any evidence of $n \geq 3$ perovskite formation (including $MAPbI_3$) as secondary phases. We attribute this lack of $n \geq 3$ formation to the favorable molecular interactions between neighboring cations in the organic layer, which lowers the formation energy of n = 1 and n = 2 phases relative to these higher n phases.[25] The MA retained in the film exists as crystalline $(PEA)_2MAPb_2I_7$ and likely also as an amorphous phase. Further deintercalation of MA out of PEA-based films can be accomplished by heating. Heating a PEA_2PbI_4 film at 100 °C after a color switch results in an initial (first 5 min) increase and redshift of the n = 1 and n = 2 absorption peaks, reflecting the recrystallization taking place. With further heating, there is a decrease in the n = 2 absorption peak, indicating MA off-gassing (Figure S1), but this peak remains clearly visible after 1 h at 100 °C, demonstrating the difficulty of complete MA deintercalation. The existence of n = 2 phase with $CH_3NH_3^+$ requires, by eq 1, that some neutral amine species also remain. It is possible that this neutral amine, phenethylamine, in this case, volatilizes from the film during this heating, leading to a permanent irreversibility.

Additionally, as with $CH_3NH_3PbI_3$, the bleached $PEA_2PbI_4 \cdot xCH_3NH_2$ films appear to remain solid only at lower x values (estimated to be $x \approx 1$ or 2 for $CH_3NH_3PbI_3 \cdot xCH_3NH_2$).[7]

https://doi.org/10.1021/acsaem.2c01352
ACS Appl. Energy Mater. 2022, 5, 12029–12038

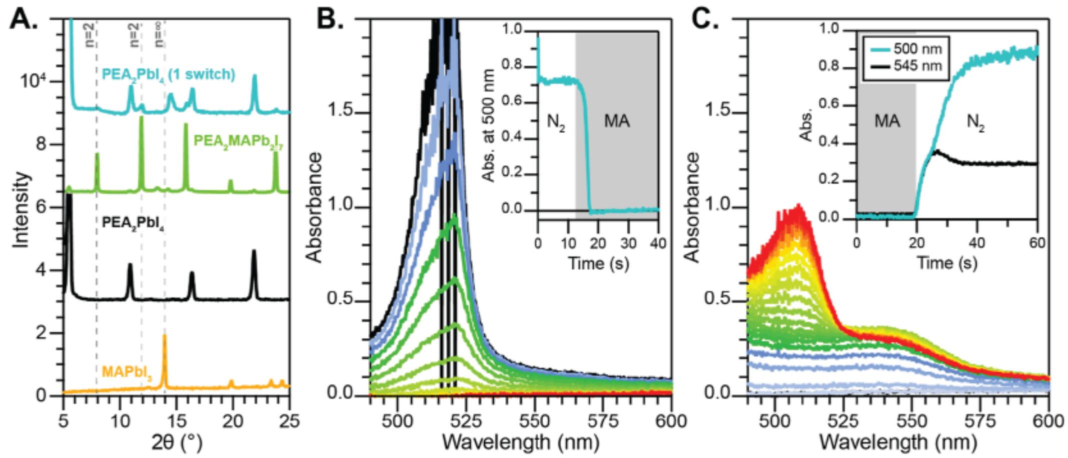

Figure 2. Methylamine intercalation−deintercalation in PEA_2PbI_4. (A) XRD patterns of (from bottom to top) $MAPbI_3$ and the as-synthesized PEA_2PbI_4 film ($n = 1$) compared to the as-synthesized $(PEA)_2MAPb_2I_7$ film and the PEA_2PbI_4 film following one color switch. Dashed vertical lines highlight the position of key scattering peaks for $n = 2$ and $n = \infty$ phases. (B) UV−visible absorbance traces taken over the course of approximately 2.3 s (6 traces/s) showing the bleaching of the PEA_2PbI_4 film. (C) Similar kinetic data showing the fast absorption recovery (6 traces/s) of the PEA_2PbI_4 film absorbance upon exposure to pure N_2. The insets shown the kinetics of the bleach/recovery, with shaded regions showing approximately when MA vapor was introduced.

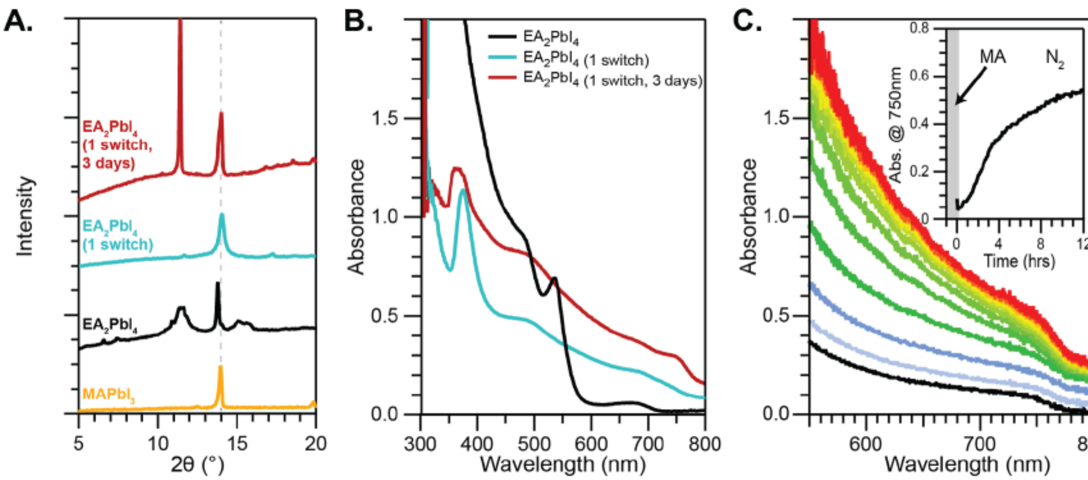

Figure 3. Methylamine intercalation−deintercalation in EA_2PbI_4. (A) XRD patterns of (from bottom to top) $MAPbI_3$ and EA_2PbI_4 films initially, immediately following 1 switch and approximately 3 days later. The dashed vertical line highlights the peak position of $MAPbI_3$ (110 peak). (B) UV−visible absorbance traces showing the absorbance of these materials shown in (A). (C) Absorption data showing the slow increase in film absorption following exposure to MA. Spectra shown were taken each hour with the kinetics at 750 nm, as shown in the inset.

Similar to what has been seen with $CH_3NH_3PbI_3$,[19,26] extended exposure to the high partial pressure of MA leads to condensation of MA and liquefaction of the film. This was achieved by placing PEA_2PbI_4 films immediately overtop a solution of MA in ethanol for various times. Short (~1 s) exposure led to qualitatively the same behavior discussed above. On the other hand, visible liquid drops were seen to form on the film surface after approximately 10 s in the solution headspace. Removal of the film from the MA gas resulted in the same behavior in cases of long and short exposure to high vapor pressure MA, but the liquefaction led to film dissolution (see photographs in Figure S2).

Solvatochromism of EA_2PbI_4 and Methylamine. To demonstrate the breadth of effects and processes with different A-site cations, a detailed discussion of the behavior of ethylammonium lead iodide films is instructive. When crystallized, films made with 2:1 EAI:PbI_2 stoichiometry lms) appear to form a previously identified one-dimensional (1D) crystalline phase with face-sharing octahedral chains, as evidenced by the broad diffraction peaks at 11.4 and 15.1°,[25] as well as one or more other crystalline phases with peaks at 7.43, 10.88, and 13.79° (this last peak is possibly attributable to some 3D $EAPbI_3$ formation), and not $n = 1$ 2D perovskite phase (Figure 3A). When exposed to MA vapor, EA_2PbI_4 films bleach similar to PEA_2PbI_4 but at lower MA exposure (Figure S3). Despite the similarity in the intercalation between EA_2PbI_4 and PEA_2PbI_4, significant differences are found for MA deintercalation. On short timescales, deintercalation of MA results in the formation of an absorption peak at 375 nm, significantly blueshifted from the absorption of EA_2PbI_4 (Figure 3B). This material is difficult to characterize because of its transience, but it contains a significant amount of trapped MA that, we hypothesize, could be a 1D iodoplumbate phase akin to hydrated $MAPbI_3$.[14,27] Over a timescale of hours, MA continues to deintercalate, and a 3D perovskite material is formed, as

https://doi.org/10.1021/acsaem.2c01352
ACS Appl. Energy Mater. 2022, 5, 12029−12038

evidenced by the growth of a new absorption peak at 750 nm (Figure 3C) and an XRD peak at 14.0°; however, the presence of the sharp XRD peak at 11.39° and the absorption peak at 365 nm show that not all of the material converts to 3D perovskite.[28] Comparing the XRD patterns of this material with that of $MAPbI_3$, this newly formed 3D perovskite has an asymmetric XRD peak ,with a shoulder at a lower angle, indicating that there is some $MA_xEA_{1-x}PbI_3$ formed (Figure S4).

At least a portion of the observed irreversibility in EA_2PbI_4 films is attributed to off-gassing of the neutral ethylamine formed by proton exchange of ethylammonium with the MA gas (eq 1). Ethylamine has a boiling point below room temperature (b.p. = 16.7 °C), making it quite volatile under the experimental conditions (room temperature). This is observed experimentally by flowing MA/N_2 gas over ethylammonium iodide powder. After continued exposure to MA (several minutes), the ethylammonium iodide powder is seen to liquefy. Upon removal of the gas flow, this liquid returns to a solid that was then analyzed by ^{1}H NMR (Figure S5). From this data, it is clear that the MA undergoes a proton exchange with ethylammonium to form methylammonium iodide and that no detectable ethylamine remains present in the remaining solid as a result of ethylamine off-gassing.

To summarize these initial experiments, the A-site cation has a marked effect on the intercalation/deintercalation of MA in A_2PbI_4 films, especially on the deintercalation process. Figure 4 attempts to show the range of materials formed, depending on the degree to which MA deintercalates from the film. Exposure of the as-synthesized films to MA gas causes the films to form a transparent, MA-intercalated phase. This is conceivably similar to what was shown by Wheeler *et al.* for $MAPbI_3$.[7] Then, when MA is removed from the film headspace, the films become colored and can reform the initial material or form an array of secondary phases (Figure 4B). The relative proportions of these secondary phases, or how reversible the MA intercalation/deintercalation process is, can be controlled by the specific A-site cation used. Based on this insight, additional work was done to investigate design criteria for the A-site cation that could enable reversible solvatochromic MHPs.

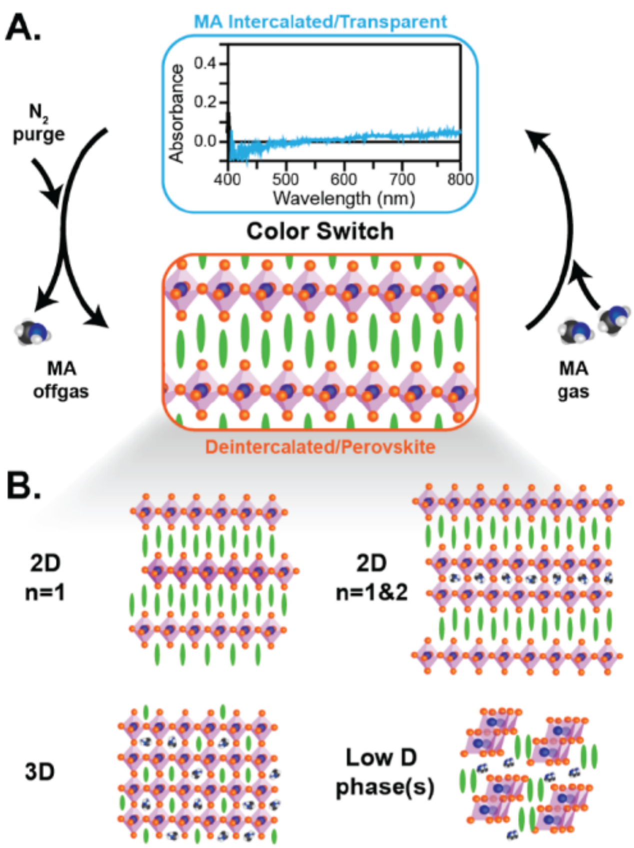

Figure 4. MA intercalation/deintercalation summary. (A) Schematic showing MA intercalation/deintercalation and the absorbance of intercalated PEA_2PbI_4, and (B) structures of some of the identified

Changing the A-Site Cation Length. From the previously discussed results, it is clear that more MA is retained in the EA_2PbI_4 films than in the PEA_2PbI_4 films. An area of difference in these two materials is the difference in the A-site cation size and, therefore, the strength of the molecular interactions. As mentioned previously, stronger interactions in the organic interlayer should favor $n = 1$ formation.[25,29] The strength of these interactions in the organic interlayer was therefore explored through a series of phenalkylammonium A-site cations $C_6H_5(C_mH_{2m})NH_3^+$ with varying chain length, m: phenylammonium (PhA, $m = 0$), phenethylammonium (PEA, $m = 2$), and phenbutylammonium (PBA, $m = 4$). Intermolecular interactions should be the weakest with PhA because the lack of a flexible carbon chain could lead to a more disordered organic layer.[10] In fact, PhA is the only one of these three cations that does not form a typical oriented $n = 1$ perovskite (Figure S6).

PhA_2PbI_4, PEA_2PbI_4, and PBA_2PbI_4 were synthesized and characterized. Each material has an absorption peak of around 515 nm (Figure 5). When PhA_2PbI_4 films go through a color switch, we see a blueshift in the absorbance spectra similar to that seen in Figure 3 with EA_2PbI_4. We attribute this to a large amount of MA being retained in the switched PhA_2PbI_4 films. As described previously, when PEA_2PbI_4 films go through a color switch, we see the reformation of the $n = 1$ phase with $n = 2$ material also present, indicating PEA leads to decreased MA retention relative to PhA. Extending the chain length and increasing intermolecular interactions further, PBA_2PbI_4 films also went through a color switch and, like PEA films, afterward show an absorption peak from an $n = 2$ phase at approximately 550 nm; however, this $n = 2$ absorbance peak decreases with time and eventually disappears. Films that were allowed to rest after switching to dry air at room temperature for 72 h no longer show an $n = 2$ phase absorbance peak and have fully reverted to the $n = 1$ phase. That said, the exciton peak is significantly decreased in intensity following this process, which is a sign of increased defect concentrations[30] arising from irreversible morphological changes in the films (Figure S7).

Tuning A-Site/Iodide Interactions in R-PEA_2PbI_4 Materials. Interactions between the organic cation and the halide perovskite sheets can also be tuned through careful selection of the A-site cations. In another set of experiments, a series of PEA cations were substituted at the 4-position on the phenyl ring to subtly control the interactions between the organic layer and the Pb−I sheet. These materials are abbreviated as R-PEA, where R = F, Cl, I, H, MeO, or HO. As shown by Knutson *et al.* with tin MHPs, and more recently seen in lead MHPs,[31,32] subtle changes in the R-group of R-PEA can introduce small changes in cation penetration and distort the Pb−I−Pb bond angle (Figure 6A). Greater cation

https://doi.org/10.1021/acsaem.2c01352
ACS Appl. Energy Mater. 2022, 5, 12029−12038

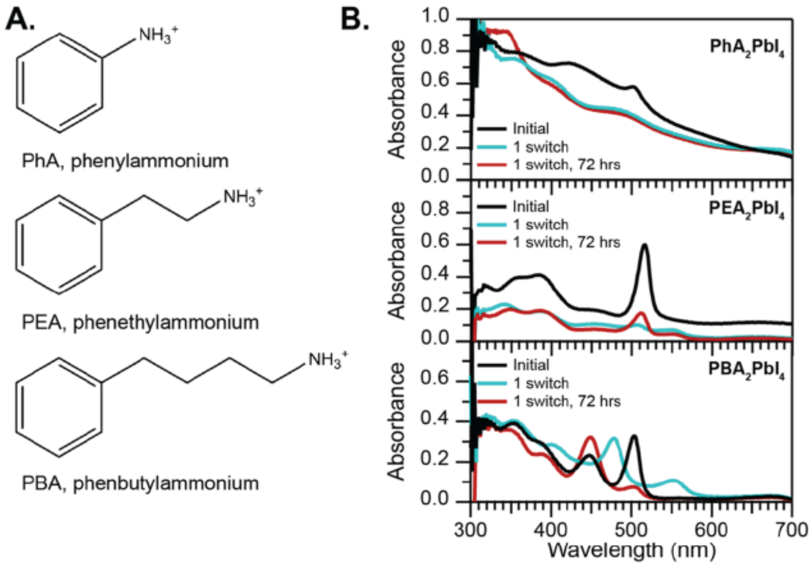

Figure 5. Intercalation with the chain length. (A) Structure of A-site cations used in A_2PbI_4 perovskites. (B) Absorbance traces of A_2PbI_4 films on FTO substrates before, immediately after, and 3 days after one switch.

penetration, caused by increased hydrogen bonding strength between the NH_3 and the axial iodides, leads to larger Pb−I−Pb bond angle distortions from 180° and causes a widening of the material's band gap.[32] Changing this interaction can also lead to octahedral distortions in the PbI_6 octahedra, but previous work has found no clear relationship between these octahedral distortions and band gap. Thus, examining the band gap of the R-PEA series can provide insights into this interaction strength with stronger interactions leading to a blueshift in the exciton absorbance peak (Figure 6B). The observed data shows very similar binding strength for F-PEA, Cl-PEA, and PEA with slightly stronger interactions for MeO-PEA and HO-PEA. This is consistent with previous structural characterization of some of these R-PEA 2D perovskites, which has found that the average Pb−I−Pb bond angles of F-PEA, Cl-PEA, and PEA were 151.405(10), 152.479(16), and 152.198(15)°, respectively.[21]

Three specific R-PEA_2PbI_4 materials were selected, F-PEA, PEA, and HO-PEA, for a more detailed study. From the exciton peak position, the interaction strength differs only slightly between these three materials and follows the trend F-PEA < PEA < HO-PEA, consistent with bond angle measurements in structural studies.[21,33] Because these differences are small along this series, we do not anticipate differences in behavior to be a result of differing cation "head"-inorganic interaction strength. As shown in Figure 6C−E, the materials underwent a color switch with MA, observed by UV-visible absorbance. Additionally, SEM images were collected for films of the same composition before and after switching. In both F-PEA and PEA, after switching, there is a significant decrease in the intensity of the $n = 1$ absorption peak and a new peak corresponding to the formation of the $n = 2$ phase. There are also readily apparent changes in the film morphology before and after switching. On the other hand, for HO-PEA, we see no formation of an $n = 2$ phase after switching along with reduced absorbance and morphological changes although these still occur.

As stated before, the absorption spectra and structural information indicate little difference in the $NH_3 \cdots I$ hydrogen

rganic "head" and the inorganic layer. Therefore, a different effect is likely to be responsible for this differing behavior. In addition to the "head"-inorganic interaction, there can also be "tail-inorganic" interactions between the cation and the next inorganic sheet. For the halogenated R-PEA cations, this has previously been investigated where it was shown that halogen bonding can occur, where the halogen on the organic cation acts as the halogen-bond donor (Lewis acid) and the iodine on the inorganic layer acts as halogen-bond acceptor (Lewis base).[21] Similar halogen bonding interactions have also been used in the charge transport layer design.[34] For the cation series studied, we anticipate weak interactions between the cation "tail" and the neighboring inorganic lattice for PEA, F-PEA, and Cl-PEA because these cations lack an appropriate electron donor. The position of the cations between the inorganic sheets, as determined from the crystal structures of these, and similar materials,[21,33] supports this idea. On the other hand, we anticipate hydrogen-bonding "tail-inorganic" interactions in HO-PEA because of the hydroxyl hydrogen. We propose that this "tail-inorganic" interaction in HO-PEA_2PbI_4 is thus largely responsible for the improved intercalation−deintercalation reversibility.

HO-PEA_2PbI_4 films display additional unique behaviors to be noted, likely also a result of the hydroxyl group. When synthesized using a mixture of DMF/DMSO as the solvent, the HO-PEA_2PbI_4 films retain a 2D perovskite structure with negligible absorbance changes but have an expanded lattice. There is a shift in the (001) reflection from 5.20 to 4.42°, corresponding to an increase in *d*-spacing of 1.5 Å (Figure S8), which we attribute to DMSO intercalation. This behavior has been shown in the pentafluorophenethylammonium compounds explored by Mitzi and co-workers.[35] The formation of this intercalated 2D perovskite structure appears to arise due to the hydrogen bonding of the hydroxyl hydrogen with DMSO. It is also worth noting that the films shown in Figure 6C−E are quite thin (stock solutions are diluted 1:10 v/v with DMF for these absorption measurements and 1:3 v/v for SEM imaging). F-PEA_2PbI_4 and PEA_2PbI_4 films show qualitatively similar behavior in thick and thin films although the formation of high-quality thick films is more challenging with all compositions

https://doi.org/10.1021/acsaem.2c01352
ACS Appl. Energy Mater. 2022, 5, 12029−12038

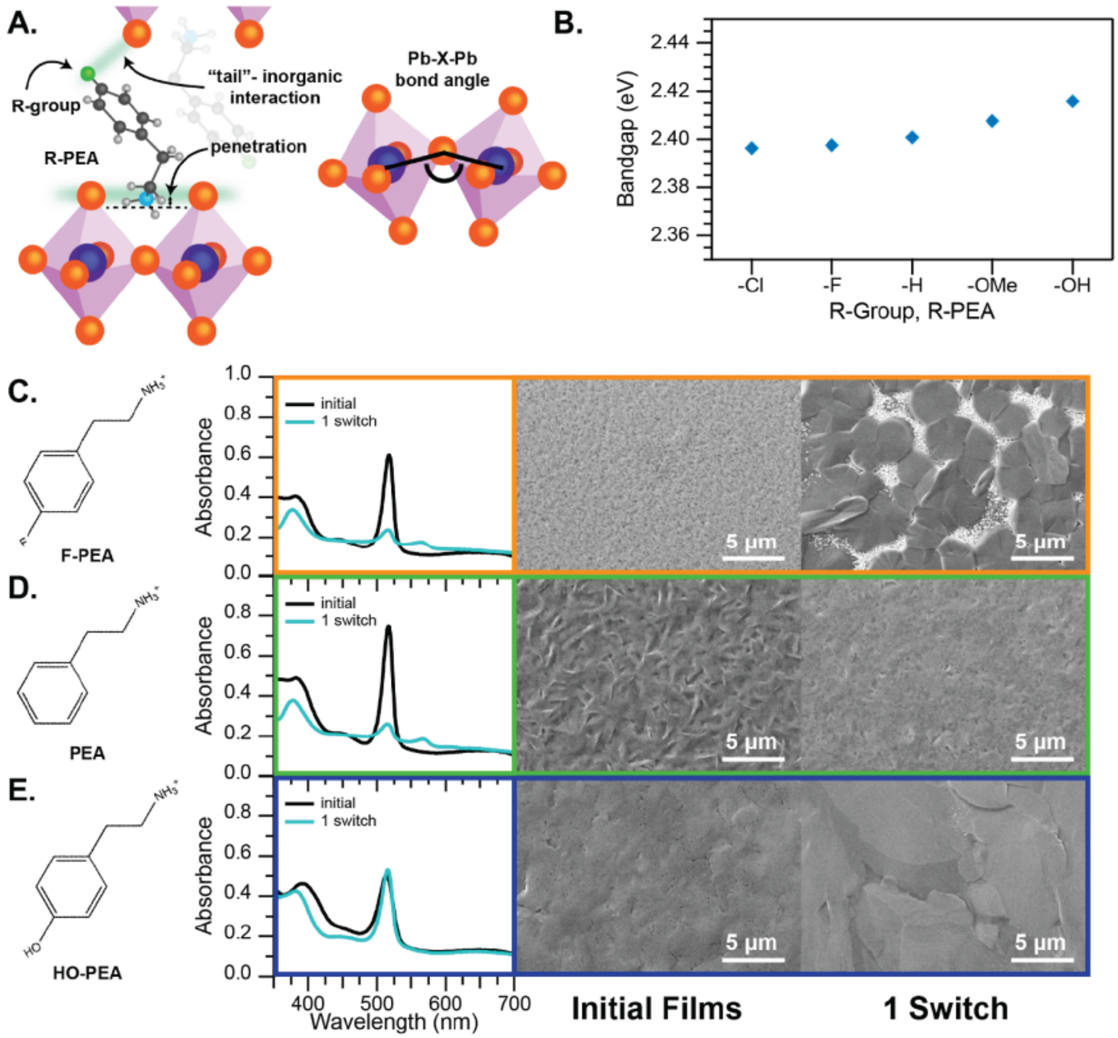

Figure 6. Intercalation/deintercalation in R-PEA_2PbI_4 materials. (A) Diagram showing how organic cation penetration into the perovskite layer can lead to Pb−I−Pb bond distortions and interactions with cation "tail" and adjacent axial halide. (B) Band gap energy calculated from the absorption excitonic peak plotted for various R-groups in R-PEA_2PbI_4 films. (C−E) Results of MA intercalation/deintercalation across three select R-PEA_2PbI_4 materials. From left to right is shown, the structure of the A-site cation, UV−visible absorbance spectra of the R-PEA_2PbI_4 film before and after one switch, and SEM images of film morphology for these materials before and after one switch.

(Figure S9). For both F-PEA_2PbI_4 and PEA_2PbI_4, as well as other materials described subsequently, switching multiple times results in a dramatic reduction of the $n = 1$ absorption peak. When HO-PEA_2PbI_4 films are switched repeatedly, there is dramatically less change in absorption and morphology (Figure S10).

To provide additional evidence for the organic "tail-inorganic" interactions proposed to be important for HO-PEA_2PbI_4, we synthesized 4-iodophenethylammonium iodide (I-PEAI) and fabricated I-PEA_2PbI_4 films. The polarizability of iodine makes it a suitable halogen-bond donor and thus able to form halogen bonds with the neighboring inorganic layer iodide.[21,34] Before synthesizing this compound, we hypothesized that the halogen-bonding of I-PEA_2PbI_4 films would lead to more reversible MA intercalation−deintercalation than F-PEA_2PbI_4 or PEA_2PbI_4 but would be less reversible than HO-PEA_2PbI_4 and its hydrogen-bonding interactions. In fact, this is what is observed (Figure S11). I-PEA_2PbI_4 films show the formation of a small amount of $n = 2$ perovskite, but this largely disappears after a few days of storage in dry air. ility of this effect is seen from the behavior of Cl-PEA_2PbI_4 and MeO-PEA_2PbI_4, which both show improved reversibility compared to F-PEA_2PbI_4 or PEA_2PbI_4 but are not as reversible as I-PEA_2PbI_4 or HO-PEA_2PbI_4 (Figure S12). This trend follows the expected trend in interaction strength between the cation "tail" and the axial iodide of the neighboring inorganic layer, moving from no interaction for PEA and F-PEA to a stronger interaction with the MeO hydrogens, halogen bonding with I-PEA, and then finally the likely hydrogen-bonding interaction with HO-PEA.

Design Rules and Additional A-Site Cation Experiments. Taken together, we hypothesize that the design of halide perovskites with reversible MA solvatochromism and less significant morphological changes can be enabled or supported by the careful selection of organic spacers. We show that this requires balancing several interactions: (i) cation−cation intermolecular interactions within the organic interlayer (and the related volatility of the neutral amine), (ii) hydrogen-bonding between the organic cation "head" and the metal halide layer, and (iii) interactions between the cation "tail" and the adjacent axial halides.

https://doi.org/10.1021/acsaem.2c01352
ACS Appl. Energy Mater. 2022, 5, 12029−12038

Building from these three design rules, we performed MA intercalation−deintercalation experiments on 2D perovskites with a number of additional A-site cations. Further evidence for the importance of cation−cation interactions is seen with *n*-pentylammonium (*n*-PA) and 4-methoxy-phenylammonium (MeO-PhA), as shown in Figures S13 and S14. Comparing *n*-PA with EA, we expect to see stronger intermolecular interactions and improved reversibility with *n*-PA because of the longer carbon chain (5 carbons *vs* 2 carbons). Indeed, *n*-PA shows an initial redshift in absorption, followed by a blueshift (low-dimensional structure, high MA-uptake) only with repeated MA exposure. EA films show this same blueshift or high MA-uptake, with only minimal MA exposure. Likewise, comparing MeO-PhA with MeO-PEA, MeO-PEA has two additional carbons and is expected to show a similar trend, as is shown in Figure 5 between PhA and PEA. This is what is observed, as shown in Figure S14. There is evidence of high MA-retention in MeO-PhA films with the formation of a low-dimensional phase, and only moderate MA-retention in MeO-PEA films with the formation of a small $n = 2$ phase absorption peak. It is important to note, in this context, as described for EA_2PbI_4, that the proton exchange reaction (eq 1) that can occur in these systems means the potential presence of neutral amines in the film. One of the reasons A-site cations with stronger intermolecular interactions lead to improved reversibility is that these same interactions lead to reduced amine volatility.

Finally, the hydrogen bonding between the cation "head" and metal halide layer can also be tuned by substituting Br for I because Br will lead to stronger hydrogen bonding with the cation ammonium. To test this, we compare reversibility between PEA_2PbI_4 and PEA_2PbBr_4. We anticipate improved reversibility with Br because of the stronger hydrogen bonding, which is what is observed (Figure S15). Switching the PEA_2PbI_4 films with MA results in the formation of an $n = 2$ absorption peak following the initial switch; however, PEA_2PbBr_4 films only show the growth of a very small $n = 2$ absorption peak after they have been switched multiple times.

The experiments discussed to this point took minimal care to reduce moisture exposure. However, to begin to uncover the role that water plays in the process, we performed additional experiments with $HO\text{-}PEA_2PbI_4$ and $I\text{-}PEA_2PbI_4$ films where moisture exposure was reduced as much as possible. In both of these cases, we see evidence for the formation of higher-dimensionality phases when moisture is excluded. $HO\text{-}PEA_2PbI_4$ then shows the formation of an $n = 2$ perovskite phase, and $I\text{-}PEA_2PbI_4$ shows an increased $n = 2$ phase and also $n = 3+$ phases (Figure S16). These films also took longer to return to a colored phase once the MA vapor was removed than they did when some moisture was present. This shows that water plays a significant role in the deintercalation process and shifts the equilibrium of eq 1. Fully understanding the role that water can play in this process is an important future challenge. As another effect worth describing, thick $HO\text{-}PEA_2PbI_4$ films show the formation of a significant amount of $MAPbI_3$ when exposed to MA gas (Figure S17), which we believe to be a result of the poor initial film quality. Additionally, it should be noted that thin $HO\text{-}PEA_2PbI_4$ films appear to be sensitive to the MA gas concentration and storage time/conditions after fabrication. These, and perhaps other variables as well, lead to variations in reversibility (Figure S18) and will require careful analysis and control in a [illegible]ased on this mechanism.

■ CONCLUSIONS

Methylamine demonstrates a rich interaction with 2D halide perovskites, and the nature of the A-site cation plays the main role in dictating the interactions. After intercalation into the structure, methylamine can become incorporated and form a variety of new impurity phases with either higher dimensionality (*e.g.*, $n = 2$ or 3D perovskites) or lower dimensionality. These secondary phases dramatically alter the material properties of the film and are therefore unwanted in a solvatochromic semiconductor system. Additionally, the long-chain ammonium cations can undergo a proton exchange reaction with MA that can, in at least some cases, lead to off-gassing of the now neutral long-chain amine. Secondary phase formation can be reduced dramatically by manipulating interlayer interactions in the organic layer and the interactions between the organic cations and lead halide sheets.

In the experiments performed in this work, morphological changes were significantly reduced but not wholly suppressed. While there is likely still significant room for further improvement, device designs centered on this chromogenic mechanism may need to accommodate both the material expansion/compression with MA intercalation/deintercalation and perhaps some morphological changes resulting from this process. Nevertheless, these initial explorations provide a roadmap for future A-site cation development to template MHPs for chromogenic applications while also providing insights into the rich interactions in 2D halide perovskites. Given this improved understanding of organic cation design rules, 2D perovskites or mixed 2D/3D perovskites are shown to be a promising material system for MHP chromogenics although significant questions remain, and much more work is required to explore this approach. Moreover, careful manipulation of cation−cation, cation "head"-inorganic, and cation "tail"-inorganic interactions will likely all prove to be important considerations for the design and stability of 2D and 2D/3D halide perovskites for a wide array of optoelectronic applications.

■ ASSOCIATED CONTENT

Supporting Information

The Supporting Information is available free of charge at https://pubs.acs.org/doi/10.1021/acsaem.2c01352.

> UV−Visible absorption experiments heating PEA_2PbI_4; photographs showing long MA exposure on films; photographs comparing PEA_2PbI_4 and EA_2PbI_4 switching; XRD pattern of EA_2PbI_4 after 1 color switch; 1H NMR spectra of the reaction between EAI and MA; XRD patterns of PhA_2PbI_4 and PBA_2PbI_4; SEM morphology of PBA_2PbI_4; XRD patterns of $HO\text{-}PEA_2PbI_4$ films fabricated with and without DMSO; UV−visible absorption experiments showing 10 color switches for PEA_2PbI_4, $F\text{-}PEA_2PbI_4$, $HO\text{-}PEA_2PbI_4$, $I\text{-}PEA_2PbI_4$, EA_2PbI_4, $n\text{-}PA_2PbI_4$, $MeO\text{-}PhA_2PbI_4$, and PEA_2PbBr_4; comparison of UV−visible absorption experiments for $R\text{-}PEA_2PbI_4$ films; water-free UV−visible absorption experiments with $HO\text{-}PEA_2PbI_4$ and $I\text{-}PEA_2PbI_4$; additional UV−visible absorption experiments with $HO\text{-}PEA_2PbI_4$ films (PDF)

https://doi.org/10.1021/acsaem.2c01352
ACS Appl. Energy Mater. 2022, 5, 12029−12038

■ AUTHOR INFORMATION

Corresponding Author

Jeffrey A. Christians − *Department of Engineering, Hope College, Holland, Michigan 49423, United States;* orcid.org/0000-0002-6792-9741; Email: christians@hope.edu

Authors

Josephine L. Surel − *Department of Engineering, Hope College, Holland, Michigan 49423, United States;* orcid.org/0000-0002-7019-1864

Elizabeth V. Cutlip − *Department of Engineering, Hope College, Holland, Michigan 49423, United States*

James R. Mandeville − *Department of Engineering, Hope College, Holland, Michigan 49423, United States*

Complete contact information is available at: https://pubs.acs.org/10.1021/acsaem.2c01352

Author Contributions

J.L.S. and E.V.C. contributed equally to this paper. J.A.C. led the project and wrote the first draft of the manuscript. J.A.C., J.L.S., E.V.C., and J.R.M. contributed to materials synthesis, data collection, and analysis. All authors edited the manuscript and have given approval for the final version.

Notes

The authors declare no competing financial interest.

■ ACKNOWLEDGMENTS

The authors acknowledge Dr. Meagan Elinski for assistance with AFM imaging and Dr. Jeffrey Johnson for assistance with NMR. Research reported in this publication was supported in part by the Hope College Dean of Natural and Applied Sciences and the Hope College Department of Engineering. J.A.C. acknowledges support from the Towsley Research Scholars Program grant from the Towsley Foundation of Midland, Michigan. E.V.C. and J.L.S. acknowledge support from the Clare Booth Luce Research Scholar program. Research reported in this publication was supported in part by funding provided by the National Aeronautics and Space Administration (NASA), under award number 80NSSC20M0124, Michigan Space Grant Consortium (MSGC). This material was supported by the National Science Foundation under Major Research Instrumentation Award No. 2117655. The authors would also like to thank the reviewers for their helpful critique and suggestions.

■ REFERENCES

(1) Manser, J. S.; Christians, J. A.; Kamat, P. V. Intriguing Optoelectronic Properties of Metal Halide Perovskites. *Chem. Rev.* **2016**, *116*, 12956−13008.

(2) Snaith, H. J. Present Status and Future Prospects of Perovskite Photovoltaics. *Nat. Mater.* **2018**, *17*, 372−376.

(3) Zhao, Y.; Zhu, K. Optical bleaching of perovskite (CH3NH3)-PbI3 through room-temperature phase transformation induced by ammonia. *Chem. Commun.* **2014**, *50*, 1605−1607.

(4) Hao, J.; Kim, Y. H.; Habisreutinger, S. N.; Harvey, S. P.; Miller, E. M.; Foradori, S. M.; Arnold, M. S.; Song, Z.; Yan, Y.; Luther, J. M.; Blackburn, J. L. Low-Energy Room-Temperature Optical Switching in Mixed-Dimensionality Nanoscale Perovskite Heterojunctions. *Sci. Adv.* **2021**, *7*, 1−12.

(5) Kim, Y. H.; Zhai, Y.; Lu, H.; Pan, X.; Xiao, C.; Gaulding, E. A.; Harvey, S. P.; Berry, J. J.; Vardeny, Z. V.; Luther, J. M.; Beard, M. C. Chiral-Induced Spin Selectivity Enables a Room-Temperature Spin 1129−1133.

(6) Kim, Y. C.; Kim, K. H.; Son, D. Y.; Jeong, D. N.; Seo, J. Y.; Choi, Y. S.; Han, I. T.; Lee, S. Y.; Park, N. G. Printable Organometallic Perovskite Enables Large-Area, Low-Dose X-Ray Imaging. *Nature* **2017**, *550*, 87−91.

(7) Wheeler, L. M.; Moore, D. T.; Ihly, R.; Stanton, N. J.; Miller, E. M.; Tenent, R. C.; Blackburn, J. L.; Neale, N. R. Switchable Photovoltaic Windows Enabled by Reversible Photothermal Complex Dissociation from Methylammonium Lead Iodide. *Nat. Commun.* **2017**, *8*, 1722.

(8) Liu, X.-K.; Xu, W.; Bai, S.; Jin, Y.; Wang, J.; Friend, R. H.; Gao, F. Metal Halide Perovskites for Light-Emitting Diodes. *Nat. Mater.* **2021**, *20*, 10−21.

(9) Saparov, B.; Mitzi, D. B. Organic-Inorganic Perovskites: Structural Versatility for Functional Materials Design. *Chem. Rev.* **2016**, *116*, 4558−4596.

(10) Li, X.; Hoffman, J. M.; Kanatzidis, M. G. The 2D Halide Perovskite Rulebook: How the Spacer Influences Everything from the Structure to Optoelectronic Device Efficiency. *Chem. Rev.* **2021**, *121*, 2230.

(11) Mitzi, D. B.; Feild, C. A.; Harrison, W. T. A.; Guloy, A. M. Conducting Tin Halides with a Layered Organic-Based Perovskite Structure. *Nature* **1994**, *369*, 467−469.

(12) Jeong, J.; Kim, M.; Seo, J.; Lu, H.; Ahlawat, P.; Mishra, A.; Yang, Y.; Hope, M. A.; Eickemeyer, F. T.; Kim, M.; Yoon, Y. J.; Choi, I. W.; Darwich, B. P.; Choi, S. J.; Jo, Y.; Lee, J. H.; Walker, B.; Zakeeruddin, S. M.; Emsley, L.; Rothlisberger, U.; Hagfeldt, A.; Kim, D. S.; Grätzel, M.; Kim, J. Y. Pseudo-halide anion engineering for α-FAPbI3 perovskite solar cells. *Nature* **2021**, *592*, 381−385.

(13) Christians, J. A.; Miranda Herrera, P. A.; Kamat, P. V. Transformation of the Excited State and Photovoltaic Efficiency of CH3NH3PbI3 Perovskite upon Controlled Exposure to Humidified Air. *J. Am. Chem. Soc.* **2015**, *137*, 1530−1538.

(14) Leguy, A. M. A.; Hu, Y.; Campoy-Quiles, M.; Alonso, M. I.; Weber, O. J.; Azarhoosh, P.; van Schilfgaarde, M.; Weller, M. T.; Bein, T.; Nelson, J.; Docampo, P.; Barnes, P. R. F. Reversible Hydration of CH3NH3PbI3 in Films, Single Crystals, and Solar Cells. *Chem. Mater.* **2015**, *27*, 3397−3407.

(15) Lin, J.; Lai, M.; Dou, L.; Kley, C. S.; Chen, H.; Peng, F.; Sun, J.; Lu, D.; Hawks, S. A.; Xie, C.; Cui, F.; Alivisatos, A. P.; Limmer, D. T.; Yang, P. Thermochromic Halide Perovskite Solar Cells. *Nat. Mater.* **2018**, *17*, 261−267.

(16) Rosales, B. A.; Mundt, L. E.; Allen, T. G.; Moore, D. T.; Prince, K. J.; Wolden, C. A.; Rumbles, G.; Schelhas, L. T.; Wheeler, L. M. Reversible Multicolor Chromism in Layered Formamidinium Metal Halide Perovskites. *Nat. Commun.* **2020**, *11*, 1−12.

(17) Wheeler, L. M.; Wheeler, V. M. Detailed Balance Analysis of Photovoltaic Windows. *ACS Energy Lett.* **2019**, *4*, 2130−2136.

(18) Halder, A.; Choudhury, D.; Ghosh, S.; Subbiah, A. S.; Sarkar, S. K. Exploring Thermochromic Behavior of Hydrated Hybrid Perovskites in Solar Cells. *J. Phys. Chem. Lett.* **2015**, *6*, 3180−3184.

(19) Bogachuk, D.; Wagner, L.; Mastroianni, S.; Daub, M.; Hillebrecht, H.; Hinsch, A. The nature of the methylamine-MAPbI3 complex: fundamentals of gas-induced perovskite liquefaction and crystallization. *J. Mater. Chem. A* **2020**, *8*, 9788−9796.

(20) Mitzi, D. B. Templating and structural engineering in organic-inorganic perovskites. *J. Chem. Soc., Dalton trans.* **2001**, *1*, 1−12.

(21) Tremblay, M. H.; Bacsa, J.; Zhao, B.; Pulvirenti, F.; Barlow, S.; Marder, S. R. Structures of (4-Y-C6H4CH2NH3)2PbI4 {Y = H, F, Cl, Br, I}: Tuning of Hybrid Organic Inorganic Perovskite Structures from Ruddlesden-Popper to Dion-Jacobson Limits. *Chem. Mater.* **2019**, *31*, 6145−6153.

(22) Smith, I. C.; Hoke, E. T.; Solis-Ibarra, D.; McGehee, M. D.; Karunadasa, H. I. A Layered Hybrid Perovskite Solar-Cell Absorber with Enhanced Moisture Stability. *Angew. Chem.* **2014**, *126*, 11414−11417.

(23) Jeon, N. J.; Noh, J. H.; Kim, Y. C.; Yang, W. S.; Ryu, S.; Seok, S. Solvent engineering for high-performance inorganic-organic hybrid perovskite solar cells. *Nat. Mater.* **2014**, *13*, 897−903.

(24) Proppe, A. H.; Johnston, A.; Teale, S.; Mahata, A.; Quintero-Bermudez, R.; Jung, E. H.; Grater, L.; Cui, T.; Filleter, T.; Kim, C. Y.; Kelley, S. O.; De Angelis, F.; Sargent, E. H. Multication Perovskite 2D/3D Interfaces Form via Progressive Dimensional Reduction. *Nat. Commun.* **2021**, *12*, 1−9.

(25) Xing, J.; Zhao, Y.; Askerka, M.; Quan, L. N.; Gong, X.; Zhao, W.; Zhao, J.; Tan, H.; Long, G.; Gao, L.; Yang, Z.; Voznyy, O.; Tang, J.; Lu, Z. H.; Xiong, Q.; Sargent, E. H. Color-Stable Highly Luminescent Sky-Blue Perovskite Light-Emitting Diodes. *Nat. Commun.* **2018**, *9*, 1−8.

(26) Zhao, T.; Williams, S. T.; Chueh, C.-C.; deQuilettes, D. W.; Liang, P.-W.; Ginger, D. S.; Jen, A. K.-Y. Design Rules for the Broad Application of Fast (<1 s) Methylamine Vapor Based, Hybrid Perovskite Post Deposition Treatments. *RSC Adv.* **2016**, *6*, 27475−27484.

(27) Hetsch, F.; Xu, X.; Wang, H.; Kershaw, S. V.; Rogach, A. L. Semiconductor Nanocrystal Quantum Dots as Solar Cell Components and Photosensitizers: Material, Charge Transfer, and Separation Aspects of Some Device Topologies. *J. Phys. Chem. Lett.* **2011**, *2*, 1879−1887.

(28) Wang, G.-E.; Wang, M.-S.; Jiang, X.-M.; Liu, Z.-F.; Lin, R.-G.; Cai, L.-Z.; Guo, G.-C.; Huang, J.-S. Crystal Structures and Optical Properties of 1-D Iodoplumbates Templated by in Situ Synthesized p-Phenylenediamine Derivatives. *Inorg. Chem. Commun.* **2011**, *14*, 1957−1961.

(29) Aharon, S.; Wierzbowska, M.; Etgar, L. The Effect of the Alkylammonium Ligand's Length on Organic-Inorganic Perovskite Nanoparticles. *ACS Energy Lett.* **2018**, *3*, 1387−1393.

(30) Fox, M. *Optical Properties of Solids*, 2nd edn.; Oxford University Press: Oxford, United Kingdom, 2010.

(31) Knutson, J. L.; Martin, J. D.; Mitzi, D. B. Tuning the Band Gap in Hybrid Tin Iodide Perovskite Semiconductors Using Structural Templating. *Inorg. Chem.* **2005**, *44*, 4699−4705.

(32) Du, K. Z.; Tu, Q.; Zhang, X.; Han, Q.; Liu, J.; Zauscher, S.; Mitzi, D. B. Two-Dimensional Lead(II) Halide-Based Hybrid Perovskites Templated by Acene Alkylamines: Crystal Structures, Optical Properties, and Piezoelectricity. *Inorg. Chem.* **2017**, *56*, 9291−9302.

(33) Straus, D. B.; Iotov, N.; Gau, M. R.; Zhao, Q.; Carroll, P. J.; Kagan, C. R. Longer Cations Increase Energetic Disorder in Excitonic 2D Hybrid Perovskites. *J. Phys. Chem. Lett.* **2019**, *10*, 1198−1205.

(34) Metrangolo, P.; Canil, L.; Abate, A.; Terraneo, G.; Cavallo, G. Halogen Bonding in Perovskite Solar Cells: A New Tool for Improving Solar Energy Conversion. *Angew. Chem., Int. Ed.* **2022**, *61*, No. e202114793.

(35) Mitzi, D. B.; Medeiros, D. R.; Malenfant, P. R. L. Intercalated Organic−Inorganic Perovskites Stabilized by Fluoroaryl−Aryl Interactions. *Inorg. Chem.* **2002**, *41*, 2134−2145.

https://doi.org/10.1021/acsaem.2c01352
ACS Appl. Energy Mater. 2022, 5, 12029−12038